CrossMark

THE SPATIAL DISTRIBUTION OF COMPLEX ORGANIC MOLECULES IN THE L1544 PRE-STELLAR CORE

IZASKUN JIMÉNEZ-SERRA[1,2,3], ANTON I. VASYUNIN[4,5], PAOLA CASELLI[4], NURIA MARCELINO[6,7], NICOLAS BILLOT[8], SERENA VITI[2],
LEONARDO TESTI[3,9], CHARLOTTE VASTEL[10,11], BERTRAND LEFLOCH[12,13], AND RAFAEL BACHILLER[14]

[1] Astronomy Unit, School of Physics & Astronomy, Queen Mary University of London, Mile End Road, London E1 4NS, UK; i.jimenez-serra@qmul.ac.uk
[2] Department of Physics & Astronomy, University College London, 132 Hampstead Road, London NW1 2PS, UK
[3] European Southern Observatory (ESO), Karl-Schwarzschild-Str. 2, D-85748 Garching, Germany
[4] Max-Planck-Institut für extraterrestrische Physik (MPE), Gießenbachstr., D-85741 Garching, Germany
[5] Ural Federal University, Ekaterinburg, Russia
[6] INAF, Osservatorio di Radioastronomia, Via P. Gobetti 101, I-40129 Bologna, Italy
[7] Instituto de Ciencia de Materiales de Madrid, CSIC, C/ Sor Juana Inés de la Cruz 3, E-28049 Cantoblanco, Spain
[8] Instituto de Radioastronomía Milimétrica, Avenida Divina Pastora 7, E-18012 Granada, Spain
[9] INAF-Osservatorio Astrofisico di Arcetri, Largo E. Fermi 5, I-50125 Firenze, Italy
[10] Université de Toulouse, UPS-OMP, IRAP, F-31400 Toulouse, France
[11] CNRS, IRAP, 9 Av. Colonel Roche, BP 44346, F-31028 Toulouse Cedex 4, France
[12] Univ. Grenoble Alpes, IPAG, F-38000 Grenoble, France
[13] CNRS, IPAG, F-38000 Grenoble, France
[14] Observatorio Astronómico Nacional (OAN, IGN), Calle Alfonso XII 3, E-28014 Madrid, Spain

ABSTRACT

The detection of complex organic molecules (COMs) toward cold sources such as pre-stellar cores (with $T < 10$ K) has challenged our understanding of the formation processes of COMs in the interstellar medium. Recent modeling on COM chemistry at low temperatures has provided new insight into these processes predicting that COM formation depends strongly on parameters such as visual extinction and the level of CO freeze out. We report deep observations of COMs toward two positions in the L1544 pre-stellar core: the dense, highly extinguished continuum peak with $A_V \geqslant 30$ mag within the inner 2700 au; and a low-density shell with average $A_V \sim 7.5$–8 mag located at 4000 au from the core's center and bright in CH_3OH. Our observations show that CH_3O, CH_3OCH_3, and CH_3CHO are more abundant (by factors of $\sim$2–10) toward the low-density shell than toward the continuum peak. Other COMs such as CH_3OCHO, c-C_3H_2O, $HCCCHO$, CH_2CHCN, and $HCCNC$ show slight enhancements (by factors $\leqslant$3), but the associated uncertainties are large. This suggests that COMs are actively formed and already present in the low-density shells of pre-stellar cores. The modeling of the chemistry of O-bearing COMs in L1544 indicates that these species are enhanced in this shell because (i) CO starts freezing out onto dust grains driving an active surface chemistry; (ii) the visual extinction is sufficiently high to prevent the UV photo-dissociation of COMs by the external interstellar radiation field; and (iii) the density is still moderate to prevent severe depletion of COMs onto grains.

Key words: astrochemistry – ISM: individual objects (L1544) – ISM: molecules – stars: formation

1. INTRODUCTION

Complex organic molecules (COMs) are carbon-based species with $\geqslant 6$ atoms in their molecular structure (Herbst & van Dishoeck 2009). The most prolific regions in the detection of COMs in the interstellar medium (ISM) have been massive hot cores and giant molecular clouds in the Galactic Center (SgrB2 (N) and (M); Hollis et al. 2000, 2006; Belloche et al. 2008, 2014; Requena-Torres et al. 2008) and low-mass hot corinos (IRAS16293-2422; Ceccarelli et al. 2000; Bottinelli et al. 2004; Jørgensen et al. 2012). Until recently, it was believed that COMs form on dust grains via hydrogenation (Charnley et al. 1995) or radical–radical reactions favored by the heating from the central protostar (at $T \geqslant 30$ K; see Garrod et al. 2008). However, the detection of COMs such as propylene (CH_2CHCH_3), acetaldehyde (CH_3CHO), dimethyl ether (CH_3OCH_3), or methyl formate (CH_3OCHO) in dark cloud cores and pre-stellar cores with $T \leqslant 10$ K (B1-b, TMC-1, L1689B, or L1544) has recently challenged our understanding of COM formation (Marcelino et al. 2007; Öberg et al. 2010; Bacmann et al. 2012; Cernicharo et al. 2012; Vastel et al. 2014; Loison et al. 2016).

Several mechanisms have been proposed to explain the presence of COMs in cold cores: gas-phase formation, non-canonical chemical explosions, cosmic-ray induced radical diffusion, impulsive spot heating of grains, or radical–radical recombination after H-atom addition/abstraction reactions on grain surfaces (Rawlings et al. 2013; Vasyunin & Herbst 2013; Reboussin et al. 2014; Balucani et al. 2015; Ivlev et al. 2015; Chuang et al. 2016). However, information about the spatial distribution of COMs in cold cores is lacking (as well as of their radial abundance profile probing different density and extinction regimes), which prevents us from testing these COM formation scenarios.

The detection of a low-density, CH_3OH-rich shell around the continuum peak of the L1544 pre-stellar core (Bizzocchi et al. 2014) offers a unique opportunity to test COM formation scenarios in cold sources. Species such as C_3O, ketene (H_2CCO), formic acid (HCOOH), and acetaldehyde may be spatially co-located to CH_3OH in L1544 and may form at this low-density shell (Vastel et al. 2014). We report high-sensitivity observations of COMs toward two positions in the L1544 pre-stellar core: the continuum peak and a position within the low-density, CH_3OH-rich shell reported by Bizzocchi et al. (2014, hereafter the *CH3OH peak*). Our results suggest that COMs are actively formed in the low-density shells of pre-stellar cores.[15]
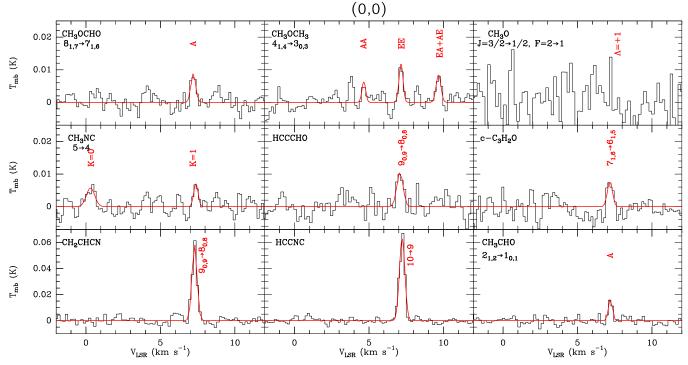

Figure 1. Sample of COM lines detected toward L1544's dust continuum peak. Red lines show the Gaussian line fits derived for the COM transitions (see Table 1). The CH_3O spectrum has been extracted from the ASAI data (Vastel et al. 2014).

2. OBSERVATIONS

High-sensitivity single-pointing 3 mm observations were carried out toward two positions in the L1544 core during 2014 December 10–16 and 2016 June 15–16 with the Instituto de Radioastronomía Milimétrica (IRAM) 30 m telescope. We pointed our observations toward the core's dust continuum peak, $\alpha(J2000) = 5^h04^m17^s.21$, $\delta(J2000) = 25° 10'42''.8$, and toward the CH_3OH peak, $\alpha(J2000) = 5^h04^m18^s$ and $\delta(J2000) = 25° 11'10''$ (Bizzocchi et al. 2014). This position is ∼30'' away from the core's center (∼0.02 pc or 4000 au at 140 pc; Elias 1978).

The observations were done in wobbler-switched mode with an angular throw of ±120''. The dual sideband (2SB) EMIR E090 receivers were tuned at 84.37 GHz and 94.82 GHz with rejections ⩾10 dB. We used three slightly different central frequencies (84.35, 84.37, 84.39 GHz and 94.80, 94.82, 94.84 GHz) to avoid the appearance of weak spurious features in the spectra. The FTS spectrometer allowed us to observe the inner part of each 4 GHz sub-bands covering 7.2 GHz in total, and it provided a spectral resolution of 50 kHz (0.15–0.18 km s^{-1} at 3 mm). The observed frequency ranges were 83.4–85.2, 86.7–88.5, 99.1–100.9, 102.4–104.2 GHz and 78.2–80.0, 81.4–83.2, 93.9–95.7, 97.1–98.9 GHz. Typical system temperatures were 70–120 K. The beam size was ∼28''–31'' between 79 and 87 GHz and ∼24''–26'' between 94 and 103 GHz. Intensities were calibrated in units of antenna temperature, T_A^*, and converted into main beam temperature, T_{mb}, by using beam efficiencies of 0.81 at 79–100 GHz and 0.78 at 103 GHz. The rms noise level was 1.6–2.8 mK for the core's center position and 2.2–3.7 mK for the CH_3OH peak.
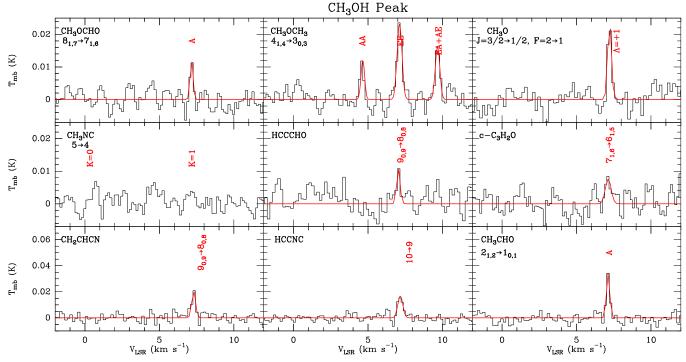
3. RESULTS

Figures 1 and 2 show some of the COM transitions detected toward L1544, while Table 1 lists all observed transitions and

their derived line parameters. For completeness, we also provide the information about the covered transitions of acetaldehyde (CH_3CHO)—species already reported by Vastel et al. (2014)—and the upper limits of formamide (NH_2CHO), methyl isocyanate (CH_3NCO), and glycine (NH_2CH_2COOH). For all COMs the spectroscopic data were extracted from the JPL catalog (Pickett et al. 1998), except for dimethyl ether (CH_3OCH_3) for which we used SLAIM[16] and cyclopropenone (c-C_3H_2O), methyl isocyanate, and glycine, for which we used the CDMS catalog (Müller et al. 2005).

Our high-sensitivity spectra reveal the detection of large COMs such as methyl formate (CH_3OCHO) and dimethyl ether (CH_3OCH_3) that had remained elusive in previous campaigns (see upper limits in Vastel et al. 2014). Other species detected are propynal (HCCCHO), cyclopropenone (c-C_3H_2O), ethynyl isocyanide (HCCNC), and vinyl cyanide (CH_2CHCN; Figures 1 and 2). Methoxy (CH_3O), considered as a COM precursor or COM dissociation product, is also detected toward the CH_3OH peak. All these molecules are observed at the ∼10–20 mK intensity level (Table 1). In Figure 1, we also report the tentative detection of methyl isocyanide (CH_3NC) toward the continuum peak. Its $K = 0,1$ lines are detected at the 2.5σ and 3.2σ level. We are confident about the correct identification of all transitions since their derived radial velocities match the v_{LSR} of the source (7.2 km s^{-1}), and for most species at least two transitions are detected. In addition, we have looked for other lines that could be blended and have found none. Since the COM line profiles are narrow (line widths ∼0.3–0.4 km s^{-1}; Table 1), it is unlikely that they appear blended with unknown species.

Table 1 shows that the line emission from O-bearing species is either brighter toward the CH_3OH peak (by factors of ∼2–3

Figure 2. As in Figure 1, but for the position of the *CH₃OH peak*.

for CH₃O, CH₃CHO, CH₃OCHO, and CH₃OCH₃) or remains constant toward both positions (HCCCHO and c-C₃H₂O). The N-bearing COMs HCCNC, CH₃NC, and CH₂CHCN, on the contrary, show an opposite behavior with brighter emission seen toward the center of the core. As shown in Section 5, this behavior translates into larger enhancements toward the *CH₃OH peak* for CH₃O, CH₃CHO, and CH₃OCH₃ than for the rest of COM species. Formamide, methyl isocyanate, and glycine are not detected toward any position in L1544 (Table 1).

4. EXCITATION ANALYSIS OF COMs

For CH₃O, CH₃OCHO, CH₃OCH₃, CH₃CHO, CH₃NC, and CH₂CHCN, we have detected several lines so that a multi-line excitation analysis can be performed. The excitation temperature, T_{ex}, and total column density, N_{obs}, of these molecules have been calculated using the MADCUBAIJ software (Martín et al. 2011; Rivilla et al. 2016), assuming extended emission and LTE conditions. Except for CH₃NC (which is tentatively detected; Section 3), the derived T_{ex} is ~5–6 K toward the core's center and ~5–8 K toward the *CH₃OH peak* (Table 2). Errors of T_{ex} in Table 2 correspond to 1σ uncertainties. We note that in some cases we had to fix T_{ex} to make MADCUBAIJ converge and find a solution. Since c-C₃H₂O is not included in MADCUBAIJ, we used the Weeds software for this molecule (Maret et al. 2011) and assumed that its emission fills the beam.

For the COMs with only one transition detected (and also for the non-detections), we again used MADCUBAIJ and assumed extended emission and a T_{ex} range of 5–10 K for both positions. This T_{ex} range agrees well with the values of T_{ex} obtained from the COM multi-line excitation analysis (Table 2) and with the T_{ex} measured from CH₃OH by Bizzocchi et al. (2014). The estimated values of N_{obs} are reported in Table 2.

5. COM ABUNDANCE PROFILES IN L1544

By calculating the COM molecular abundances toward the two positions in L1544, we can provide constraints to the COM abundance profiles as a function of radius within the core. For the continuum peak, we need to calculate the H₂ column density, $N(H_2)$, within a radius of 13″ or 1900 au (i.e., half the IRAM 30 m beam of our observations). The $N(H_2)$ of the core for radii $\leqslant$2500 au (~18″ at 140 pc) is nearly flat with a radius dependence $N(H_2) \propto r^{-0.8}$ (Ward-Thompson et al. 1999). By using the peak $N(H_2)$ obtained by Crapsi et al. (2005; 9.4×10^{22} cm^{-2}) for a radius of 6″5 (~910 au), we derive that $N(H_2) = 5.4 \times 10^{22}$ cm^{-2} for a radius of 13″ (1900 au). This value is similar to that estimated by Bacmann et al. (2000) for the same radius (4.5×10^{22} cm^{-2}; see their Table 2). The slight difference is due to the dust temperatures assumed in both calculations (12.5 K in Bacmann et al. 2000 versus 10 K in Crapsi et al. 2005). Hereafter, we use $N(H_2) = 5.4 \times 10^{22}$ cm^{-2} for the position of the continuum peak within a radius of 13″.

For the *CH₃OH peak*, we assume an H₂ column density of 1.5×10^{22} cm^{-2} as derived by Spezzano et al. (2016) from Herschel data. The latter $N(H_2)$ corresponds to a visual extinction A_V ~15–16 mag using the Bohlin et al. (1978) formula. We note, however, that the model of L1544 by Keto & Caselli (2010) and Keto et al. (2014) considers the extinction as a function of radius (within the core and not along the line of sight) and therefore the modeled A_V at this position is about half that measured along the line of sight ($A_V \sim 7.5$–8 mag; see also Section 7).

From Table 2 and Figure 3 (lower panel), we find that CH₃O, CH₃OCH₃, and CH₃CHO are enhanced respectively by factors $\geqslant$4–5, ~2, and ~10 in the *CH₃OH peak* with respect to L1544's center (note that their associated 1σ uncertainties are lower than these enhancements). The other O-bearing COMs CH₃OCHO, c-C₃H₂O, and HCCCHO show average abundances slightly higher toward the *CH₃OH peak* than toward the

4

Table 1
COM Transitions Covered in Our Observations and Their Derived Line Parameters

Species	Line	Frequency (MHz)	E_u (K)	g_u	A_{ul} (s^{-1})	(0″,0″) Area[a] (mK km s^{-1})	V_{LSR} (km s^{-1})	Δv (km s^{-1})	T_{mb}[b] (mK)	CH$_3$OH Peak Area[a] (mK km s^{-1})	V_{LSR} (km s^{-1})	Δv (km s^{-1})	T_{mb}[b] (mK)
CH$_3$O[c]	$F = 1 \to 0, \Lambda = -1$	82455.98	4.0	3	6.5×10^{-6}	⩽3.7	…	…	⩽16.2	3.5(0.9)	7.06(0.03)	0.3(0.1)	10.8(2.4)
	$F = 2 \to 1, \Lambda = -1$	82458.25	4.0	5	9.8×10^{-6}	⩽3.7	…	…	⩽15.9	9.2(1.1)	7.21(0.02)	0.40(0.05)	21.8(3.0)
	$F = 2 \to 1, \Lambda = +1$	82471.82	4.0	5	9.8×10^{-6}	⩽3.9	…	…	⩽17.1	7.8(1.0)	7.22(0.02)	0.30(0.05)	24.3(2.9)
	$F = 1 \to 0, \Lambda = +1$	82524.18	4.0	3	6.5×10^{-6}	⩽3.5	…	…	⩽15.0	2.6(0.9)	7.14(0.06)	0.27(0.08)	8.9(3.0)
CH$_3$OCHO	$9_{1,9} \to 8_{1,8}$ E	100078.608	25.0	38	1.4×10^{-5}	1.8(0.8)	7.23(0.10)	0.42(0.2)	4.1(2.0)	⩽1.7	…	…	⩽8.1
	$9_{1,9} \to 8_{1,8}$ A	100080.542	25.0	38	1.4×10^{-5}	2.0(1.0)	7.22(0.19)	0.44(0.15)	4.4(1.7)	3.3(0.8)	7.16(0.03)	0.30(0.09)	10.4(2.6)
	$8_{3,5} \to 7_{3,4}$ E	100294.604	27.4	34	1.3×10^{-5}	⩽1.3	…	…	⩽5.4	3.5(0.9)	7.20(0.04)	0.34(0.10)	9.9(2.5)
	$8_{3,5} \to 7_{3,4}$ A	100308.179	27.4	34	1.3×10^{-5}	⩽1.7	…	…	⩽7.2	⩽1.4	…	…	⩽6.9
	$8_{1,7} \to 7_{1,6}$ E	100482.241	22.8	34	1.4×10^{-5}	⩽4.1	…	…	⩽5.7	6.5(0.9)	7.17(0.02)	0.31(0.06)	19.6(2.7)
	$8_{1,7} \to 7_{1,6}$ A	100490.682	22.8	34	1.4×10^{-5}	3.5(0.7)	7.21(0.04)	0.37(0.07)	8.9(2.2)	3.0(0.7)	7.16(0.03)	0.23(0.06)	12.3(2.6)
	$9_{0,9} \to 8_{0,8}$ E	100681.545	24.9	38	1.5×10^{-5}	1.6(0.9)	7.16(0.11)	0.4(0.2)	4.1(2.8)	⩽1.6	…	…	⩽7.5
	$9_{0,9} \to 8_{0,8}$ A	100683.368	24.9	38	1.5×10^{-5}	4.1(1.1)	7.12(0.07)	0.54(0.14)	7.2(2.7)	3.3(0.7)	7.11(0.03)	0.24(0.05)	13.1(2.6)
CH$_3$OCH$_3$	$4_{1,4} \to 3_{0,3}$ EA[d]	99324.357	10.2	36	2.2×10^{-5}	3.4(0.8)	7.11(0.05)	0.38(0.10)	8.4(2.4)	6.2(1.2)	7.11(0.03)	0.36 (0.08)	16.4(3.5)
	$4_{1,4} \to 3_{0,3}$ AE[d]	99324.359	10.2	54	3.3×10^{-5}	…	…	…	…	…	…	…	…
	$4_{1,4} \to 3_{0,3}$ EE	99325.208	10.2	144	8.9×10^{-5}	4.0(0.8)	7.15(0.03)	0.32(0.07)	11.55(2.2)	9.6(1.2)	7.12(0.02)	0.39(0.06)	23.5(3.1)
	$4_{1,4} \to 3_{0,3}$ AA	99326.058	10.2	90	5.5×10^{-5}	2.0(0.9)	7.22(0.09)	0.3(0.2)	5.4(2.5)	3.7(1.1)	7.12(0.05)	0.29(0.09)	12.0(3.7)
	$6_{2,5} \to 6_{1,6}$ EA[d]	100460.412	24.7	52	1.8×10^{-5}	⩽1.2	…	…	⩽5.8	⩽1.8	…	…	⩽7.8
	$6_{2,5} \to 6_{1,6}$ AE[d]	100460.437	24.7	78	2.6×10^{-5}	…	…	…	…	…	…	…	…
	$6_{2,5} \to 6_{1,6}$ EE	100463.066	24.7	208	7.0×10^{-5}	⩽1.2	…	…	⩽5.7	1.4(0.8)	7.16(0.07)	0.26(0.16)	5.2(2.6)
	$6_{2,5} \to 6_{1,6}$ AA	100465.708	24.7	130	4.4×10^{-5}	⩽1.3	…	…	⩽6.3	⩽1.8	…	…	⩽7.8
CH$_3$CHO	$2_{1,2} \to 1_{0,1}$ E	83584.260	5.0	10	2.2×10^{-6}	3.8(1.5)	7.12(0.04)	0.32(0.10)	10.9(2.6)	12.8(1.1)	7.18(0.01)	0.31(0.04)	39.0(3.1)
	$2_{1,2} \to 1_{0,1}$ A	84219.764	5.0	10	2.4×10^{-6}	5.5(0.8)	7.21(0.02)	0.30(0.05)	17.4(2.5)	9.6(0.9)	7.12(0.01)	0.26(0.02)	34.4(3.0)
	$2_{1,1} \to 1_{0,1}$ E	87109.504	5.2	10	1.3×10^{-7}	⩽1.4	…	…	⩽6.5	⩽1.7	…	…	⩽7.7
	$2_{2,0} \to 3_{1,3}$ A	87146.655	11.8	10	2.9×10^{-7}	⩽1.3	…	…	⩽6.2	⩽1.5	…	…	⩽6.6
	$2_{2,0} \to 3_{1,3}$ E	87204.278	11.9	10	1.1×10^{-7}	⩽1.6	…	…	⩽5.9	⩽1.7	…	…	⩽7.4
	$6_{3,4} \to 7_{2,5}$ A	99141.294	24.4	10	7.1×10^{-7}	⩽1.4	…	…	⩽6.7	1.8(0.8)	6.95(0.03)	0.2(0.2)	8.1(3.0)
	$6_{3,4} \to 7_{2,6}$ E	99490.149	24.3	10	6.1×10^{-7}	⩽1.4	…	…	⩽6.7	2.9(0.9)	7.33(0.07)	0.4(0.1)	6.3(2.3)
CH$_3$NC	$5_0 \to 4_0$	100526.541	14.5	44	8.1×10^{-5}	4.0(1.0)	7.15(0.09)	0.66(0.18)	5.7(2.3)	⩽1.8	…	…	⩽7.5
	$5_1 \to 4_1$	100524.249	21.5	44	7.8×10^{-5}	2.6(0.7)	7.38(0.05)	0.35(0.11)	7.0(2.2)	⩽1.8	…	…	⩽7.5
	$5_2 \to 4_2$	100517.433	42.7	44	6.8×10^{-5}	⩽1.7	…	…	⩽6.9	⩽1.8	…	…	⩽7.5
c-C$_3$H$_2$O	$6_{1,6} \to 5_{1,5}$[e]	79483.520	14.6	39	5.1×10^{-5}	…	…	…	…	7.7(1.4)	7.09(0.03)	0.38(0.08)	18.8(3.0)
	$7_{1,6} \to 6_{1,5}$	103069.925	21.1	45	1.1×10^{-4}	3.3(0.9)	7.18(0.06)	0.39(0.09)	8.0(2.8)	3.7(1.7)	7.1(0.1)	0.5(0.3)	7.6(3.4)
CH$_2$CHCN	$9_{0,9} \to 8_{0,8}$	84946.000	20.4	57	4.9×10^{-5}	24.78(1.0)	7.290(0.007)	0.397(0.019)	58.7(2.3)	6.6(1.1)	7.30(0.02)	0.29(0.06)	21.1(3.1)
	$9_{1,8} \to 8_{1,7}$	87312.812	23.1	57	5.3×10^{-5}	13.2(0.9)	7.245(0.012)	0.35(0.03)	35.3(2.4)	5.1(1.1)	7.20(0.06)	0.46(0.09)	10.4(2.7)
	$11_{0,11} \to 10_{0,10}$	103575.395	29.9	69	9.0×10^{-5}	7.8(0.8)	7.30(0.02)	0.42(0.05)	17.3(2.3)	⩽1.8	…	…	⩽8.7
HCCNC	$10 \to 9$[f]	99354.250	26.2	63	4.6×10^{-5}	29.2(1.0)	7.227(0.005)	0.438(0.013)	62.7(1.6)	7.1(1.0)	7.17(0.03)	0.40(0.05)	16.5(2.2)
HCCCHO	$9_{0,9} \to 8_{0,8}$	83775.842	20.1	19	1.8×10^{-5}	5.5(1.2)	7.08(0.06)	0.49(0.11)	10.6(2.8)	3.2(1.2)	7.04(0.06)	0.28(0.12)	10.8(3.5)
NH$_2$CHO	$4_{0,4} \to 3_{0,3}$[g]	84542.400	10.2	11	4.1×10^{-5}	⩽1.8	…	…	⩽8.4	⩽2.3	…	…	⩽9.6
	$4_{1,3} \to 3_{1,2}$[g]	87848.915	13.5	11	4.3×10^{-5}	⩽1.3	…	…	⩽6.0	⩽1.8	…	…	⩽7.2

Table 1
(Continued)

Species	Line	Frequency (MHz)	E_u (K)	g_u	A_{ul} (s^{-1})	(0″,0″) Area[a] (mK km s^{-1})	V_{LSR} (km s^{-1})	Δv (km s^{-1})	T_{mb}[b] (mK)	CH$_3$OH Peak Area[a] (mK km s^{-1})	V_{LSR} (km s^{-1})	Δv (km s^{-1})	T_{mb}[b] (mK)
CH$_3$NCO	$10_{1,10} \rightarrow 9_{1,9}$	87506.605	29.0	21	3.0×10^{-5}	⩽1.1	…	…	⩽5.1	⩽1.2	…	…	⩽5.7
	$12_{-1,12} \rightarrow 11_{-1,11}$	103023.61	39.4	25	4.9×10^{-5}	⩽1.3	…	…	⩽6.3	⩽1.6	…	…	⩽7.5
Glycine	$6_{5,2} \rightarrow 5_{4,1}$	103294.648	15.2	39	1.6×10^{-6}	⩽1.7	…	…	⩽8.0	⩽2.1	…	…	⩽9.9
Conf I.	$6_{5,1} \rightarrow 5_{4,2}$	103297.993	15.2	39	1.6×10^{-6}	⩽1.7	…	…	⩽8.0	⩽2.1	…	…	⩽9.9

Notes.

[a] Upper limits calculated as $3\sigma \times \sqrt{\Delta v \times \delta v}$, with σ the rms noise level, Δv the line width, and δv the velocity resolution of the spectrum.

[b] The rms noise level, σ, is given in parenthesis. Upper limits to the peak intensities refer to the 3σ noise level.

[c] Hyperfine components of the $N = 1-0$, $K = 0$, $J = 3/2 \rightarrow 1/2$ transition of CH$_3$O.

[d] The AE and EA transitions overlap. We only show the Gaussian fit for one of the lines. In the rotational diagram of this species, the individual areas of the AE and EA transitions are calculated by weighting the blended area by the degeneracy $g_u \times g_i$ of every transition.

[e] Transition not observed toward the continuum peak.

[f] Hyperfine structure not resolved.

[g] Hyperfine transitions blended. Spectroscopic information provided only for the brightest hyperfine component $F = 5 - 4$.

Table 2
Excitation Temperatures, Column Densities, and Measured and Modeled Abundances of COMs in L1544

Species	(0″,0″)				CH$_3$OH Peak			
	T_{ex} (K)	N_{obs} (cm^{-2})	χ_{obs}[a]	χ_{mod}[b]	T_{ex} (K)	N_{obs} (cm^{-2})	χ_{obs}[a]	χ_{mod}[b]
CH$_3$O	5–10[c]	$\leqslant(2.8–3.6)\times10^{11}$	$\leqslant(5.1–6.7)\times10^{-12}$	7.7×10^{-11}	8.0[d]	4.0×10^{11}	2.7×10^{-11}	1.3×10^{-10}
CH$_3$OCHO	5.1 ± 2.3[e]	$(4.4\pm4.0)\times10^{12}$[e]	$(8.1\pm7.4)\times10^{-11}$	8.0×10^{-11}	7.9 ± 3.6	$(2.3\pm1.4)\times10^{12}$	$(1.5\pm0.9)\times10^{-10}$	1.2×10^{-10}
CH$_3$OCH$_3$	5.7 ± 3.1	$(1.5\pm0.2)\times10^{12}$	$(2.8\pm0.4)\times10^{-11}$	8.0×10^{-11}	7.6 ± 3.7	$(7.7\pm1.6)\times10^{11}$	$(5.1\pm1.1)\times10^{-11}$	1.0×10^{-10}
CH$_3$CHO	5.0[d]	1.2×10^{12}	2.2×10^{-11}	4.0×10^{-11}	7.8[d]	3.2×10^{12}	2.1×10^{-10}	8.0×10^{-11}
CH$_3$NC	22.9[d]	2.7×10^{10}	5.0×10^{-13}	...	5–10[c]	$\leqslant(0.7–1.6)\times10^{10}$	$\leqslant(0.5–1.1)\times10^{-12}$	...
c-C$_3$H$_2$O[f]	5–10[c]	$(1.0–3.5)\times10^{11}$	$(1.9–6.5)\times10^{-12}$	...	8.0[d]	7.0×10^{10}	4.7×10^{-12}	...
CH$_2$CHCN	5.8 ± 0.9	$(1.2\pm0.8)\times10^{12}$	$(2.2\pm1.5)\times10^{-11}$	...	5.0 ± 1.4	$(5.8\pm4.7)\times10^{11}$	$(3.9\pm3.1)\times10^{-11}$	...
HCCNC	5–10[c]	$(0.3–3.0)\times10^{12}$	$(0.6–5.6)\times10^{-11}$	...	5–10[c]	$(1.0–9.1)\times10^{11}$	$(0.7–6.1)\times10^{-11}$	...
HCCCHO	5–10[c]	$(1.8–6.3)\times10^{11}$	$(0.3–1.2)\times10^{-11}$	...	5–10[c]	$(1.6–5.8)\times10^{11}$	$(1.1–3.9)\times10^{-11}$	...
NH$_2$CHO	5–10[c]	$\leqslant(1.3–1.7)\times10^{10}$	$\leqslant(2.4–3.1)\times10^{-13}$	5.0×10^{-11}	5–10[c]	$\leqslant(1.0–1.3)\times10^{10}$	$\leqslant(6.7–8.7)\times10^{-13}$	7.0×10^{-11}
CH$_3$NCO	5–10[c]	$\leqslant(0.8–6.3)\times10^{11}$	$\leqslant(0.2–1.2)\times10^{-11}$	...	5–10[c]	$\leqslant(0.9–6.3)\times10^{11}$	$\leqslant(0.6–4.2)\times10^{-11}$	...
Glycine	5–10[c]	$\leqslant(3.3–5.8)\times10^{12}$	$\leqslant(0.6–1.1)\times10^{-10}$	...	5–10[c]	$\leqslant(4.2–9.5)\times10^{12}$	$\leqslant(2.8–6.3)\times10^{-10}$	...

Notes.

[a] Molecular abundances calculated by using an H$_2$ column density of 5.4×10^{22} cm^{-2} for the continuum peak (see Section 5 for details) and of 1.5×10^{22} cm^{-2} for the position of the *CH$_3$OH peak* (Spezzano et al. 2016).
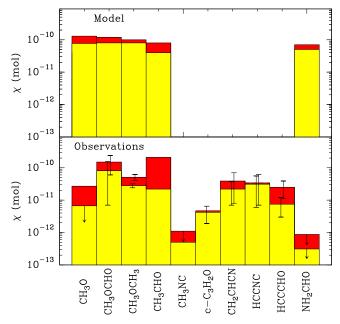
[b] Abundances predicted by the model of A. I. Vasyunin et al. (2016, in preparation).

[c] T_{ex} range assumed to calculate the total column densities from a single COM transition using MADCUBAIJ.

[d] Fitting solutions could only be obtained by fixing T_{ex} within MADCUBAIJ.

[e] Errors correspond to 1σ uncertainties in MADCUBAIJ.

[f] T_{ex} and N_{obs} calculated using Weeds.

Figure 3. Comparison of the observed and modeled abundance of COMs toward the continuum peak (in yellow) and the *CH₃OH peak* (in red; see Section 5). The abundances shown for c-C$_3$H$_2$O, HCCNC, and HCCCHO are average values. Error bars correspond to 1σ uncertainties for CH$_3$OCHO, CH$_3$OCH$_3$, and CH$_2$CHCN, while they refer to the lower/upper abundance values estimated for c-C$_3$H$_2$O, HCCNC, and HCCCHO (Table 2). Arrows indicate upper limit abundances.

core center (by factors $\leqslant 3$), although they agree within the uncertainties. The same applies to the N-bearing COMs CH$_2$CHCN, CH$_3$NC, and HCCNC, whose abundances lie within the uncertainties (Figure 3).

6. UPPER LIMITS TO THE ABUNDANCE OF PRE-BIOTIC COMs

The high-sensitivity spectra obtained toward L1544 allow us to provide stringent upper limits to the abundance of pre-biotic COMs such as glycine, NH$_2$CHO, and CH$_3$NCO. As shown in Table 2, the derived upper limits to the column density of glycine are factors of 40–120 lower than the best upper limits obtained toward the Galactic Center ($\leqslant 4 \times 10^{14}$ cm^{-2}; Jones et al. 2007). Our most stringent upper limit to the abundance of glycine in L1544 ($\leqslant 6 \times 10^{-11}$; Table 2) is also a factor of 5 lower than that inferred for the outer envelope of IRAS16293-2422 ($\leqslant 3 \times 10^{-10}$; Ceccarelli et al. 2000). Stacking analysis of the glycine lines with similar expected intensities in our frequency setup would reduce the rms noise level by a factor of ~ 3 (10 lines are covered), which implies an upper limit of $\leqslant 2 \times 10^{-11}$. This upper limit is close to the glycine abundance assumed by Jiménez-Serra et al. (2014) for the detectability of this molecule in pre-stellar cores ($\sim 3 \times 10^{-11}$). The upper limits derived for NH$_2$CHO ($\leqslant (2.4-8.7) \times 10^{-13}$) and CH$_3$NCO ($\leqslant (0.2-4.2) \times 10^{-11}$; Table 2) are consistent with those measured in L1544 and B1-b by López-Sepulcre et al. (2015; $\leqslant 5 \times 10^{-13}$) and Cernicharo et al. (2016; $\leqslant 2 \times 10^{-12}$), respectively.

7. CHEMICAL MODELING OF O-BEARING COMs

In Section 5, we have reported abundance enhancements by factors of ~ 2–10 for CH$_3$O, CH$_3$OCH$_3$, and CH$_3$CHO as a function of distance in L1544. Other COMs such as

CH$_3$OCHO may also be enhanced at larger radii, although its derived abundances agree within the uncertainties (Section 5). In this section, we model the chemistry of O-bearing COMs[17] in L1544 by using the 1D physical structure derived by Keto & Caselli (2010) and Keto et al. (2014).

We use the chemical code of Vasyunin & Herbst (2013), which considers that COMs are formed via gas-phase ion–neutral and neutral–neutral reactions after the release of precursor molecules from dust grains via chemical reactive desorption. This code has been updated with a new multilayer treatment of ices, an advanced treatment of reactive desorption based on the experiments by Minissale et al. (2016), and new gas-phase reactions proposed by Shannon et al. (2013) and Balucani et al. (2015). The complete results from this modeling will be reported in A. I. Vasyunin et al. (2016, in preparation).

The chemical evolution of COMs is followed over 3×10^6 years toward 129 points along the radius of the core to a distance of $\sim 65{,}500$ au. For all these positions, the density, temperature and A_v are taken from Keto et al. (2014). The initial molecular abundances are calculated by simulating the chemistry of a translucent cloud with density $n(H) = 10^2$ cm^{-3} and $T_{gas} = T_{dust} = 20$ K over 10^6 years. The initial atomic abundances are the same as those of Vasyunin & Herbst (2013).

Our model shows that the abundances of COMs such as CH$_3$OCHO and CH$_3$OCH$_3$ change dramatically with time reaching maximum values at 10^5–3×10^5 years. The gas-phase COM radial profiles show their peak abundances at ~ 4000 au, which roughly coincides with the position of the CH$_3$OH peak (Bizzocchi et al. 2014). In our model, this is the location where CO starts freezing out onto dust grains and it agrees well with the distance where CO depletion is observed in L1544 (see the drop in C^{17}O reported by Caselli et al. 1999). The CO depletion enhances the production of COM precursors on grain surfaces via hydrogenation reactions while, at the same time, the visual extinction is sufficiently high ($A_V \sim 7.5$–8 mag; Section 5) to prevent the UV photo-dissociation of the chemically desorbed COM precursors by the external interstellar radiation field. UV photo-desorption is not efficient at this position in the core and, therefore, the release of COMs into the gas phase is dominated by chemical reactive desorption. Toward the center of the core, the abundances of COMs drop to undetectable levels ($\leqslant 10^{-14}$) as a result of the severe freeze out.

To compare the model results with our observations, one needs to sample all COM material along the line of sight toward the continuum and the CH$_3$OH peaks. The amount of COM material sampled in the direction of the CH$_3$OH peak will be larger than toward the continuum peak. While toward the core's center COMs are found within a shell $R_{i-1} - R_i$ (with R the radius from the center and i the position in the grid with $i = 1$ at the outermost shell), toward the CH$_3$OH peak COMs are sampled along a circle chord. For the core's center the COM column density, N(COM), is given by

$$N(\text{COM}) = 2 \times \sum_{i=2}^{n} \left[\frac{n(H)_i * \chi_i + n(H)_{i-1} * \chi_{i-1}}{2} \right] \times (R_{i-1} - R_i) \tag{1}$$

with $n(H)_i$ the gas density at radial point i, χ_i the COM abundance, $(R_{i-1} - R_i)$ the shell width, and n the number of

_____

[17] Except NH$_2$CHO, none of the N-bearing COMs reported here are currently included in the chemical network of A. I. Vasyunin et al. (2016, in preparation).

shells in the model ($n = 129$). Toward the *CH₃OH peak*, N(COM) is calculated as

$$N(\text{COM}) = 2 \times \sum_{i=2}^{n_{\text{peak}}} \left[\sqrt{R_{i-1}^2 - R_{\text{peak}}^2} - \sqrt{R_i^2 - R_{\text{peak}}^2} \right]$$
$$\times \left[\frac{n(H)_i * \chi_i + n(H)_{i-1} * \chi_{i-1}}{2} \right] \quad (2)$$

where R_{peak} is the radial distance of the *CH₃OH peak* (4000 au), n_{peak} is the radial point closest to this peak, and R_i and R_{i-1} are the radii at positions i and $i - 1$. N(COM) are averaged over the beam of the IRAM 30 m telescope ($\sim 26''$), and the COM abundances are finally calculated by dividing the average N(COM) by the $N(H_2)$ obtained following the same method (4.0×10^{22} cm^{-2} for the continuum peak and 1.0×10^{22} cm^{-2} for the *CH₃OH* peak). Note that these values are similar to those used in Section 5. The best match with the observations is obtained at 10^5 years.

Table 2 and Figure 3 (upper panel) report the predicted abundances of CH₃O, CH₃OCHO, CH₃OCH₃, CH₃CHO, and NH₂CHO. The rest of O-bearing species (c-C₃H₂O, HCCCHO, CH₃NCO, and glycine) are currently not included in the chemical network and their predictions are thus not reported. The modeled COM abundances reproduce the enhancements of CH₃OCH₃ and CH₃OCHO observed toward the *CH₃OH peak* within factors of 3 (Table 2 and Figure 3). For CH₃CHO, however, the model predicts a smaller enhancement than observed, although the modeled and observed CH₃CHO abundances agree within factors of 2–3 for both positions (see Table 2). Large discrepancies are found for CH₃O and NH₂CHO (by factors of $\sim$5–15 and $\sim$100–200, respectively; Table 2), which suggests that additional mechanisms are required to supress the production of these COMs in our model.

In summary, we report new detections of COMs in L1544. Species such as CH₃O, CH₃CHO, and CH₃OCH₃ are enhanced by factors of $\sim$2–10 toward the *CH₃OH peak* with respect to the core's center. Other COMs such as CH₃OCHO may also be enhanced with increasing distance within the core (by factors $\leqslant$3), although their abundance uncertainties are large. Despite the discrepancies found between the observed COM abundances and those predicted in our model, O-bearing COMs are predicted to present an abundance peak at 4000 au, which agrees well with the position of the *CH₃OH peak* and with the radial distance at which CO depletion is observed. All this shows that high-sensitivity observations of COMs are strongly needed to put stringent constraints on chemical models and to step forward in our understanding of COM chemistry in the ISM.

REFERENCES

Bacmann, A., André, P., Puget, J.-L., et al. 2000, A&A, 361, 555
Bacmann, A., Taquet, V., Faure, A., Kahane, C., & Ceccarelli, C. 2012, A&A, 541, L12
Balucani, N., Ceccarelli, C., & Taquet, V. 2015, MNRAS, 449, L16
Belloche, A., Garrod, R. T., Müller, H. S. P., & Menten, K. M. 2014, Sci, 345, 1584B
Belloche, A., Menten, K. M., Comito, C., et al. 2008, A&A, 482, 179
Bizzocchi, L., Caselli, P., Spezzano, S., & Leonardo, E. 2014, A&A, 569A, 27B
Bohlin, R. C., Savage, B. D., & Drake, J. F. 1978, ApJ, 224, 132B
Bottinelli, S., Ceccarelli, C., Neri, R., et al. 2004, ApJ, 615, 354
Caselli, P., Keto, E., Bergin, E. A., et al. 2012, ApJL, 759, L37
Caselli, P., Walmsley, C. M., Tafalla, M., Dore, L., & Myers, P. C. 1999, ApJL, 523, L165
Ceccarelli, C., Loinard, L., Castets, A., Tielens, A. G. G. M., & Caux, E. 2000, A&A, 357, L9C
Cernicharo, J., Kisiel, Z., Tercero, B., et al. 2016, A&A, 587, L4C
Cernicharo, J., Marcelino, N., Roueff, E., et al. 2012, ApJL, 759, L43
Charnley, S. B., Kress, M. E., Tielens, A. G. G. M., & Millar, T. J. 1995, ApJ, 448, 232
Chuang, K.-J., Fedoseev, G., Ioppolo, S., van Dishoeck, E. F., & Linnartz, H. 2016, MNRAS, 455, 1702
Crapsi, A., Caselli, P., Walmsley, C. M., et al. 2005, ApJ, 619, 379
Elias, J. H. 1978, ApJ, 224, 132B
Garrod, R. T., Weaver, S. L. W., & Herbst, E. 2008, ApJ, 682, 283
Herbst, E., & van Dishoeck, E. F. 2009, ARA&A, 47, 427H
Hollis, J. M., Lovas, F. J., & Jewell, P. R. 2000, ApJL, 540, L107
Hollis, J. M., Remijan, A. J., Jewell, P. R., & Lovas, F. J. 2006, ApJ, 642, 933H
Ivlev, A. V., Röcker, T. B., Vasyunin, A., & Caselli, P. 2015, ApJ, 805, 59
Jiménez-Serra, I., Testi, L., Caselli, P., & Viti, S. 2014, ApJL, 787, L33
Jones, P. A., Cunningham, M. R., Godfrey, P. D., & Cragg, D. M. 2007, MNRAS, 374, 579
Jørgensen, J. K., Favre, C., Bisschop, S. E., et al. 2012, ApJL, 757, L4
Keto, E., & Caselli, P. 2010, MNRAS, 402, 1625
Keto, E., Rawlings, J., & Caselli, P. 2014, MNRAS, 440, 2616
Loison, J.-C., Agúndez, M., Marcelino, N., et al. 2016, MNRAS, 456, 4101
López-Sepulcre, A., Jaber, A. A., Mendoza, E., et al. 2015, MNRAS, 449, 2438
Marcelino, N., Cernicharo, J., Agúndez, M., et al. 2007, ApJL, 665, L127
Maret, S., Hily-Blant, P., Pety, J., Bardeau, S., & Reynier, E. 2011, A&A, 526, 47
Martín, S., Krips, M., & Martín-Pintado, J. 2011, A&A, 527A, 36M
Minissale, M., Moudens, A., Baouche, S., Chaabouni, H., & Dulieu, F. 2016, MNRAS, 458, 2953
Müller, H. S. P., Schlöder, F., Stutzki, J., & Winnewisser, G. 2005, JMoSt, 742, 215
Öberg, K. I., Bottinelli, S., Jorgensen, J. K., & van Dishoeck, E. F. 2010, ApJ, 716, 825O
Pickett, H. M., Poynter, R. L., Cohen, E. A., et al. 1998, JQSRT, 60, 883
Rawlings, J. M. C., Williams, D. A., Viti, S., & Cecchi-Pestellini, C. 2013, MNRAS, 430, 264
Reboussin, L., Wakelam, V., Guilloteau, S., & Hersant, F. 2014, MNRAS, 440, 3557
Remijan, A. J., Markwick-Kemper, A. & ALMA Working Group on Spectral Line Frequencies 2007, BAAS, 39, 963
Requena-Torres, M. A., Martín-Pintado, J., Martín, S., & Morris, M. R. 2008, ApJ, 672, 352
Rivilla, V. M., Fontani, F., Beltrán, M. T., et al. 2016, ApJ, 826, 161
Shannon, R. J., Blitz, M. A., Goddard, A., & Heard, D. E. 2013, NatCh, 5, 745
Spezzano, S., Bizzocchi, L., Caselli, P., Harju, J., & Brünken, S. 2016, A&A, 592, L11
Vastel, C., Ceccarelli, C., Lefloch, B., & Bachiller, R. 2014, ApJL, 795, L2
Vasyunin, A. I., & Herbst, E. 2013, ApJ, 769, 34
Ward-Thompson, D., Motte, F., & Andre, P. 1999, MNRAS, 305, 143